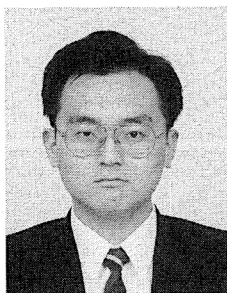
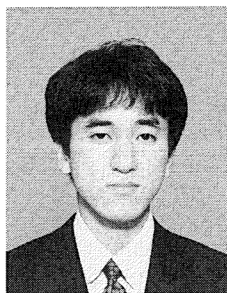


NUMERICAL SIMULATION ON CORROSION OF STEEL IN CONCRETE STRUCTURES UNDER
CHLORIDE ATTACK

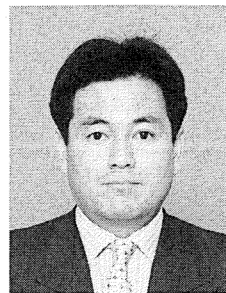
(Translation from Proceedings of JSCE, No.655/V-48, August 2000)



Kai-Lin HSU



Hitoshi TAKEDA



Tsuyoshi MARUYA

A comprehensive numerical system is proposed in an attempt to solve problems related to the deterioration of reinforced concrete (RC) structures under chloride-induced corrosion. This numerical system is characterized by combining physico-chemical models describing migration of corrosion-related substances in concrete, such as chloride, oxygen, and moisture, with electrochemical models dealing with the formation of natural potential and corrosion current in RC members under chloride-induced corrosion. An experimental comparison demonstrates the availability of this numerical system for the modeling of steel corrosion in concrete structures under chloride attack.

Keywords: *mass migration, macrocell corrosion, durability, concrete deterioration, chloride attack*

Kailin Hsu is a research engineer in Civil Material Engineering Section of Civil Engineering Research Institute of Technology Center of Taisei Corporation, Yokohama, Japan. He obtained his Ph.D. from University of Tokyo in 1997. His research interests relate to durability design and deterioration prediction of concrete structures. He is a member of JSCE.

Hitoshi Takeda is a research engineer in Civil Material Engineering Section of Civil Engineering Research Institute of Technology Center of Taisei Corporation, Yokohama, Japan. His research interests relate to durability and rehabilitation of reinforced concrete structures. He is a member of JSCE.

Tsuyoshi Maruya is a senior research engineer in Civil Material Engineering Section of Civil Engineering Research Institute of Technology Center of Taisei Corporation, Yokohama, Japan. He obtained his Doctor of Engineering degree from University of Tokyo in 1995. His research interests include the evaluation and protection of reinforced concrete structures subjected to corrosion, and prediction of the service life of concrete structures. He is a member of JSCE.

1. INTRODUCTION

According to a proposal by Miyagawa¹⁾ *et al.* the process of deterioration and degradation of concrete structures exposed to a corrosive environment can be classified into four stages: incubation period, propagation period, acceleration period, and deterioration period. As indicated in a review article by Takewaka²⁾ *et al.*, Of research related to this classification, certain observations are implied by this. First, models describing the deterioration process during the incubation period are believed to be quantitatively reliable. Secondly, according to the distribution of corrosion-related substances around rebars in concrete and the assumed models for corrosion propagation, the amount of corrosion products and the likely time until corrosion-induced cracking may be qualitatively predictable. As for predicting structural and durability performance during the acceleration and deterioration periods, little research has so far been published. On the other hand, to the authors' knowledge, although the hypothetical models adopted in research work aimed at describing the deterioration process in the propagation period are rational, they are generally so simplified that the essence of the corrosion mechanism under a corrosive environment is missed. This failing means that these research efforts lack the ability to reflect the features of steel in the process of being corroded (e.g. natural potential or polarization resistance), as often adopted in assessing the corrosion behavior of steel in concrete.

As a result, the motivation for this research is to supplement work to date by proposing electrochemical models that can properly describe the dynamic process of corrosion in concrete structures under a corrosive environment. A comprehensive numerical system that achieves this is proposed. This new numerical system is first explained in terms of its constituent models related to the transport of corrosion-related substances such as chlorides, oxygen, and moisture, respectively. Then, electrochemical models for simulating the formation of natural potential and corrosion current density are further clarified. Finally, an experimental verification is implemented to verify that this system for modeling the corrosion of steel in concrete structures under chloride attack is adequate or not. Additionally, some discussion of the parameters considered in this numerical system is included for the purpose of clarifying their influence on the numerical system.

2. DESCRIPTION OF COMPUTATIONAL MODELS

2.1 Models for Transport of Corrosion-related Substances

It is well known that the initiation of steel corrosion in concrete is strongly related to the soundness of the passivation film on the steel surface. If this passivation film is lost, it is believed that the corrosion process is initiated, i.e. the incubation period comes to an end. The substances related to the destruction of passivation films in concrete are generally regarded as chloride ions, moisture, oxygen, and carbon dioxide, etc. By integrating the past work of the authors on the transport of corrosion-related substances in concrete with that of other researchers, a single numerical system has been constructed by the authors³⁾. The computational flow for this system is illustrated in Fig.1. For a

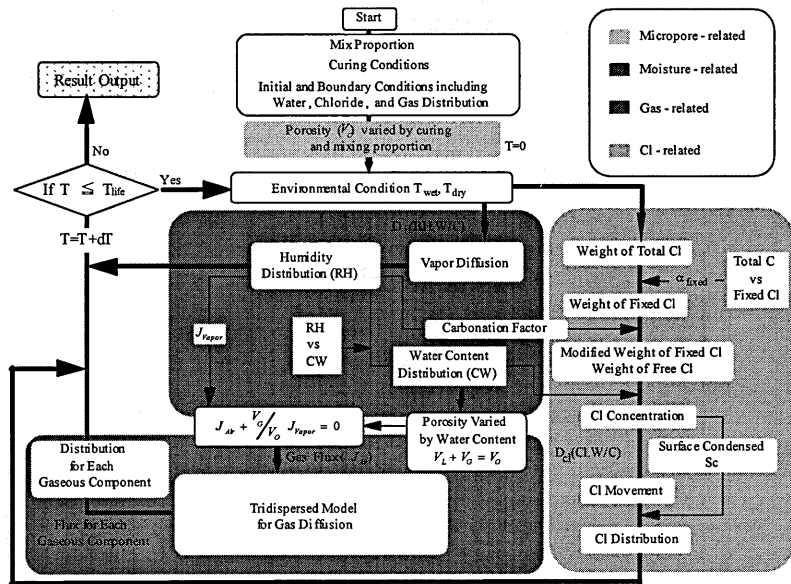


Fig.1 Computational Flow for Simulation of Transport of Corrosion-related Substances in Concrete

given mix proportion, curing conditions and environmental conditions, the model proposed by Shimomura and Maekawa⁴⁾ is adopted to trace the real-time relationship between pore structure and moisture. As for simulating moisture migration in concrete, the work of Saeki⁵⁾ *et al.* is utilized. Furthermore, by coupling the micropore structure model with moisture migration model, the real-time porosity in a wet state (V_G , cm^3/cm^3) and the volume of liquid-phase water per unit volume (V_L , cm^3/cm^3) can be traced by vapor migration simulation. Then, to simulate the migration of gaseous components in the concrete, a model proposed by Hsu⁶⁾ *et al.* is adopted. This model utilizes the usual concept of equimolar counter diffusion for a constant pressure system. By adopting this concept, their model assumes the inward flux of air (J_{Air} , $\text{cm}^3/(\text{cm}^2\text{-day})$) into the free space of pores should be equal to the outward flux of vapor (J_{Vapor} , $\text{cm}^3/(\text{cm}^2\text{-day})$) from the free space. In addition, the vapor gain due to evaporation and loss due to condensation, which are implicitly included in the calculated outflux of vapor according to the empirical model⁵⁾ used for simulation of vapor migration in concrete, are included in their model is suggested as follows:

$$J_{Air} + \frac{V_G}{V_O} \cdot J_{Vapor} = 0 \quad (1)$$

Generally speaking, the concepts of porosity and tortuosity need to be introduced into models of gas (or vapor) diffusion through porous solids, as in the micromechanical model established by Shimomura and Maekawa⁴⁾. In Eq.(1), tortuosity is considered to be implicitly included in empirical calculation of vapor migration, while porosity is reflected in the simulation of the real-time pore structure as described in the preceding models. The work of many researchers has led to a gradual understanding of the complexity of chloride diffusion in concrete and there difficulty in determining the chloride distribution merely by applying diffusion theory. The factors giving rise to this complexity are generally taken to be the equilibrium between free and fixed chlorides, the effect of carbonation, the effect of cyclic wetting and drying, as well as the condensation effect in the surface layer. Among the existing models, the mathematical model proposed by Maruya⁷⁾ *et al.* is adopted here because it is successful in integrating all these factors. However, as the work of Maruya⁷⁾ *et al.* gives no consideration to the relationship between porosity, temperature, and diffusivity of chlorides, reference is also made to the work of Saetta⁸⁾ *et al.* Through the above models, the real-time transport and accumulation of corrosion-related substances in concrete can be simulated throughout the service life (T_{life}) of a structure. The environmental conditions referred to in Fig.1 are T_{wet} (the duration of cyclic wetting) and T_{dry} (the duration of cyclic drying).

2.2 Models for Steel Corrosion in Concrete

It is well known that once corrosion due to chloride attack begins, loss of structured performance starts. The degree of structured degradation depends on the corrosion rate. Before corrosion cracks form, degradation is comparatively light, but once corrosion cracks appear, the process accelerates. In view of the electrochemistry of corrosion, performance degradation can be related to corrosion rate, which is given in the form of current density. There are three state-of-the-art approaches⁹⁾ used by researchers to model the corrosion rate: 1) models in the form of empirical relations; 2) models related to the diffusion-limited process of oxygen; and 3) models based on electrochemistry. As compared with models based on approach 1) or 2), those using approach 3) are comparatively complicated. However, it seems that they attract greater research interest despite the complexity. The reason for this is that not only can the steel corrosion rate be rationally simulated by this approach, but also the other features of steel in the process of being corroded, such as natural potential and polarization resistance. Since the natural potential (or polarization resistance) is commonly used to assess the corrosion state of steel in actual concrete during onsite measurements, this is of considerable interest. Hence, based on an understanding of the electrochemical processes of corrosion, models aimed at modeling not only the corrosion rate but also natural potential are proposed by the authors¹⁰⁾. The characteristics of these models are briefly explained below.

a) Kinetics of rebar corrosion reactions

To facilitate the interpretation that follows, a brief of the kinetics of corrosion reactions is given here. As is well known, the high alkalinity of concrete ($\text{pH} \geq 12$) protects reinforcing steel from corrosion through the formation of a passivation film. However, low alkalinity and/or a high chloride content at the steel surface can cause the passivation film to break down. Owing to the difference in potential between anode and cathode, iron is oxidized to ferrous ions at the anode and oxygen is consumed due to the release of hydroxyl ions at the cathode. The half reactions for these processes are as follows:

Anodic reaction (metal dissolution as Fe^{2+} ions)



Cathodic reaction (oxygen reduction)



By assuming that the polarization of each half-cell reaction is a simplified adaptation of Butler-Volmer kinetics, the relationship between potential and current density can be expressed as:

$$\text{Anode: } E_a = E_{a0} + \beta_a \log(i_a/i_{a0}) \quad (3.a)$$

$$\text{Cathode: } E_c = E_{c0} + \beta_c \log(i_c/i_{c0}) \quad (3.b)$$

where a and c: anode and cathode; E: potential; E_{x0} : equilibrium potential at x (i.e. a or c); β_x : activation Tafel slope for x; i_x : current density for x and i_{x0} : exchange current density for x. As Fig.2 shows, the equilibrium potential for anode and cathode reactions is termed the corrosion potential (E_{corr}) and the corresponding current density at this potential is called the corrosion current density (i_{corr}). Customarily, the measured corrosion potential of steel in concrete is often known as the natural potential, because it can also be considered the being-interacted state of the steel under natural environment.

b) Pitting potential

As commonly observed, chloride corrosion in concrete usually occurs in the form of pitting corrosion. The fall in pitting potential of concrete is related to a fall in concrete pH and/or a gain in chloride concentration. According to the two-step initiation theory of pitting corrosion suggested by Okada¹¹⁾, the pitting initiation potential (E_{pit}) can be considered as a function of pH and chloride concentration. A similar relation was reported in empirical work by Bird¹²⁾ *et al.*, as follows:

$$E_{pit} = -0.015 - 0.31 \log([Cl^-] \sqrt{[OH^-]}) \quad (\text{Vs. SCE}) \quad (4)$$

where $[OH^-]$: hydroxyl ion (M) and $[Cl^-]$: free Cl^- ion (M). Besides the influence of pH and chloride concentration, it is commonly understood that many factors, including the pore structure and water content, also affect the pitting potential; however, to maintain the simplicity of this numerical system, only the effects of pH and chloride concentration are considered, and the variation of concrete pH is assumed to be constant during the simulation.

c) Threshold chloride value

In order to destroy the passivation film, it is thought that a certain chloride concentration leading to pit initiation must exist, and this is followed by the occurrence of a perturbation, accumulation of chloride ions at local anodic sites, and then nucleus formation at the passivation film surface. As for the details of this process, reference is made to the "two-step initiation theory" suggested by Okada¹¹⁾. The critical chloride concentration is usually termed the chloride threshold value. At present, the exact expression of chloride threshold value is still under argument, for a variety of reasons, such as the difficulty in clearly understanding the real-time state of a rebar surface and the state of adhesion along the interface between rebar and concrete, etc. Nevertheless, to preserve the integrity and simplicity of this numerical system, a simple expression in terms of threshold $Cl^-:OH^-$ ratio is adopted for the moment by neglecting these effects. The expression adopted here is given by regression analysis on the results of limited experiments carried out by the authors, the details of which are given in Section 3 (Verification) of this paper. During the verification experiments, the minimum of total chloride concentration was found and converted into a free chloride ion count according to the work of Maruya⁷⁾ *et al.* Because it is impossible to measure pH during such experiments, a constant pH value in the concrete is assumed; this is the same value as used in Eq.(4). Then the threshold $Cl^-:OH^-$ ratio is determined, as follows.

$$[Cl^-] \sqrt{[OH^-]} = 4.7 \quad (5)$$

In the review work by Glass and Buenfeld¹³⁾, it is mentioned that the threshold $Cl^-:OH^-$ ratio determined for pore solutions expressed from concrete, mortar, and cement paste specimens vary more widely. For example, Yonezawa¹⁴⁾ *et al.* showed that the threshold $Cl^-:OH^-$ ratio might range from 1 to 40. Lambert¹⁵⁾ *et al.* reported that the ratio between 3 and 20 are required to initiate corrosion. These results indicate that the threshold $Cl^-:OH^-$ ratio given in Eq.(5) is within an acceptable range. It is noteworthy that the value given in Eq.(5) is only used for numerical reference rather than for practical reference in judging the start of corrosion because of its over-simplicity.

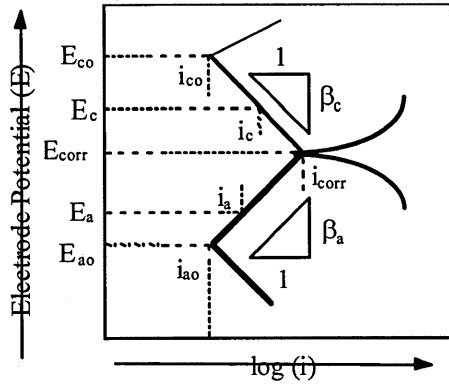


Fig.2 Polarization Model for Corrosion

d) Model for microcell potential

The term “microcell” here is adopted under the assumption that the development of the polarized potential at separate electrode (i.e. the point at the surface of rebar) is independent without the interaction between separate electrodes. If there is no pitting corrosion, the microcell potential can be regarded as the measured natural potential in the passive state. If we observe the anodic and cathodic polarization curves as schematized in Fig.3, it is found that, under sufficient access of oxygen, curve A depicts the case of no existence of Cl⁻. The intersection (i.e. $E_{microcell}$, microcell potential) of curves A (or A₁, A₂, and A₃) and B must be located between E_{trans} (transpassive potential) and E_{pass} (passive potential). With increasing Cl⁻, the corresponding E_{pit} value gradually drops. However, before reaching the threshold value of Cl⁻ (curve A₁), there is little of this fall on the formation of $E_{microcell}$. In addition, once the chloride threshold value is exceeded (curve A₃), $E_{microcell}$ is much lower than the corresponding E_{pit} . In other words, if E_{pit} is lower than the cathodic potential (E_c) at passive current density (i_{pass}), pitting corrosion is initiated. Based on this understanding, the determination of $E_{microcell}$ can be achieved by comparing the relative location of E_c and E_{pit} . This comparison can lead to a judgment of the initiation of pitting corrosion. In addition, if the Nernst equation is applied to the anodic reaction, the corresponding microcell current density ($i_{microcell}$) can be calculated.

e) Activation polarization

In the previous section, under the assumption that there exists no interaction between separate electrodes, an algorithm for calculating $E_{microcell}$ of a rebar under chloride corrosion is presented. However, once pitting corrosion is initiated, interaction between separate electrodes is possible due to the polarization. As a result, a model for macrocell corrosion is established by assuming the formation of a macrocell as the interaction between separate electrodes. According to the assumption used in the previous section, after the formation of microcell potential, the separate electrodes should be regarded as stable since no interaction takes place between them. However, once interaction between the separate electrodes is taken into account, activation polarization is required to generate the essential activation energy needed in the corrosion reactions. As illustrated in Fig.4, for any two electrodes, once pitting corrosion is initiated, the macrocell current density (i_{corr} , unit: A/cm²) can be calculated by solving the following nonlinear equation:

$$\begin{aligned}
 & E_{ma,c} - E_{ma,a} \\
 &= (L_{ac} \omega) i_{corr} \\
 &= (E_{mi,c} + \beta_{c1} \log(i_{corr} / i_{mi,c})) - \\
 & \quad (E_{mi,a} + \beta_{a2} \log(i_{corr} / i_{mi,a}))
 \end{aligned} \tag{6}$$

where ma: macrocell; mi: microcell; L_{ac} : distance between anode and cathode (cm); and ω : concrete resistivity

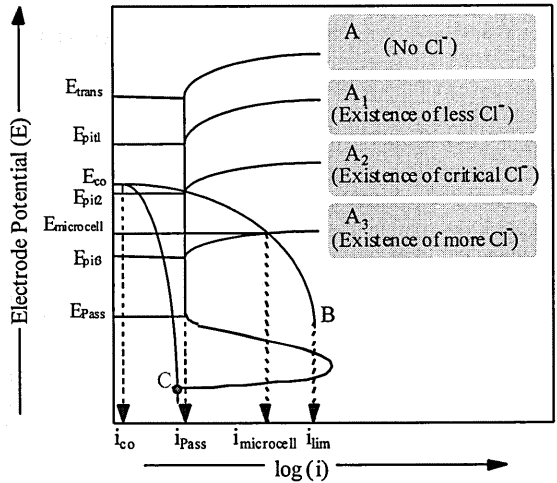


Fig.3 Model for Microcell Potential

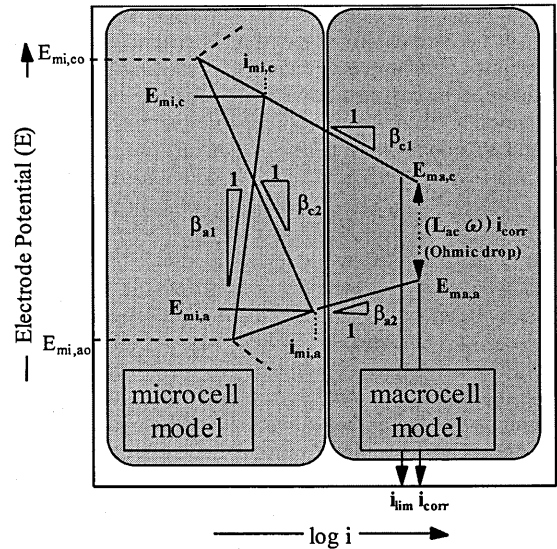


Fig.4 Model for Macrocell Potential

(Ω -cm). For the Tafel slope (i.e. β_{a2} and β_{c1}), the empirical expressions reported by the Japan Concrete Institute (JCI) committee on concrete structure repair methods¹⁶⁾ are adopted for compatibility with RC structures. These are given as follows:

$$\beta_{a2} = -0.012139 \ln(Cl^-) + 0.1916 \quad (\text{V/decade}) \quad (6.a)$$

$$\beta_{c1} = -0.037379 \ln(Cl^-) + 0.2597 \quad (\text{V/decade}) \quad (6.b)$$

where Cl^- : concentration of free chloride ions per unit volume (lb/m^3). Generally, it is thought that not only the concentration of chloride ions but also the mix proportion (e.g. the type of cement), the environment in the vicinity of the rebar (e.g. the water content), and other factors influence the Tafel slope (i.e. β_{a2} and β_{c1}). The proper empirical expression for the Tafel slope should take the above effects into consideration; however, in the literature, there seems as yet no way to consider the effects of all these factors. Once such a method becomes available, the empirical expressions given in Eq.(6.a) and (6.b), which merely consider the effect of chloride ion concentration, should be modified to suit. In order to solve the above nonlinear equation (Eq.(6)), the method of false position is utilized. Here, i_{corr} is solved so that, for the anode, the value of i_{corr} is negative to indicate the inflow of current while for the cathode i_{corr} is positive to indicate the outflow of current.

f) Limit current density

Due to the concrete cover thickness, degree of concrete saturation, and environmental conditions, the ingress of O_2 at the surface of the passivation film may be limited, which renders the corrosion reaction diffusion-limited. Furthermore, if this lack of O_2 supply is severe, the formatted potential may be even lower than E_{pass} , see point C in Fig.3. This phenomenon is often observed for RC structures submerged in the sea. In this paper, the limit current density of O_2 (i_{lim} , A/cm^2) suggested by JCI¹⁶⁾ is adopted as follows:

$$i_{lim} = \frac{M}{2.591 \times 10^{-6}} \quad (7)$$

where M : the supply flux of O_2 at the surface of a rebar in the concrete ($mol/(s\text{-}cm^2)$).

g) Model for macrocell current density

As noted, the model schematized in Fig.4 is valid for any two electrodes once pitting corrosion is initiated. However, there are usually many electrodes distributed along any rebar. That is to say, for any electrode, there should exist multiple electrical circuits. To obtain the net current density within these multiple electrical circuits, the following steps are taken:

Step 1. For N electrodes along the rebar, the number of the possible electrical circuits is $1/2N(N-1)$. By applying Eq.(6) to all possible electrical circuits, the anodic and cathodic current density for each circuit can be obtained. In other words, there is no need to specify the location of the anode and cathode (or the area ratio of the anode with respect to the cathode) before the calculation, i.e. they will be specified automatically by the exposure environment.

Step 2. By integrating the macrocell current density (i_{corr}) at each electrode along the rebar, the net macrocell current density at each electrode can be calculated as follows:

$$i_{corr,net} = \int_0^L i_{corr} dx \quad (8)$$

where $i_{corr,net}$: net macrocell current density (unit: A/cm); and L : length of the rebar.

Step 3. By the sign convention of $i_{corr,net}$, the corresponding electrode can be judged as an anode (if sign < 0) or cathode (if sign > 0).

Through the above steps, $i_{corr,net}$ at each electrode can be determined. The following equation is then utilized to convert the calculated $i_{corr,net}$ (A/cm) to an amount of Fe ¹⁶⁾ corrosion:

$$W\{Fe\} = (3987.594/r) \cdot i_{corr,net} \quad (9)$$

where $W\{Fe\}$: amount of corroded Fe ($mg/(cm^2\text{-}day)$); and r : radius of the rebar (cm). Moreover, the corrosion depth can also be calculated using the following equation:

$$h\{Fe\} = (T \cdot W\{Fe\})/\rho \quad (10)$$

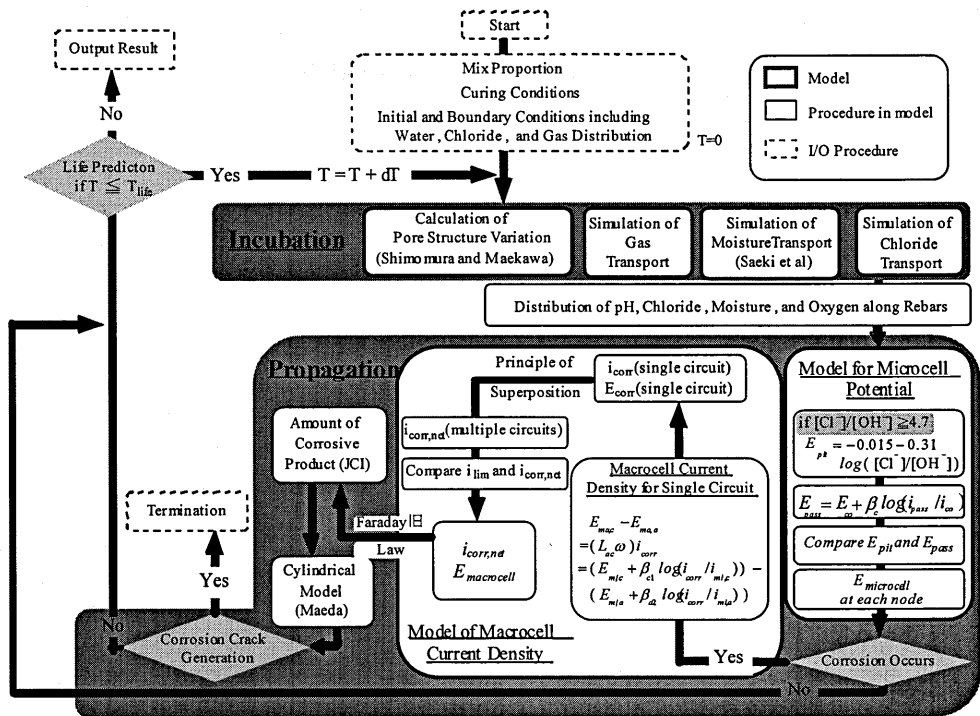


Fig.5 Computational Flow for Simulation of Incubation and Propagation Period

where $h\{Fe\}$: the corrosion depth of (cm); T : duration of corrosion (days); and p : the density of Fe ($=7860 \text{ mg/cm}^3$).

h) Model for macrocell (natural) potential

As can be observed in Fig.4, the microcell potential at a separate electrode is polarized due to activation and/or concentration (i.e. diffusion-limited) polarization. Through the above model, the existence of multiple electric circuits leads to the possibility of different polarizations for an electrode, but this contradicts the reality of the measured natural potential of the rebar.

Consequently, there is a need to modify the calculated macrocell (natural) potential. However, up to now, there has been little research on how the process of the polarization on a rebar should be. Here, by taking the average polarization of the electrode for its simplicity, the calculated macrocell (natural) potential is suitably modified. Then, the distribution of macrocell (natural) potential along the rebar can be calculated.

i) Critical corrosive depth

In order to judge whether the propagation period has come to an end or not, the criterion used is usually the corrosion depth Δx (cm), which indicates the initiation of corrosion cracking. According to a review report by a JCI committee¹⁷⁾, several proposals have been made for calculating the critical corrosion depth, such as one by Maeda¹⁸⁾, a proposal that considers restrained displacement, and one that considers volumetric expansion, etc. Of these, the Maeda's method is based on elastic theory and it is adopted here for its simplicity and ability to give predictions of suitable accuracy. Once the corrosion depth in Eq.(10) exceeds the critical corrosion depth, the simulation process mentioned in this paper is terminated, since the simulation of corrosion cracks is not the focus of this paper.

j) Integration of models for simulation

Following by the explanations on the characteristics of the electrochemical model, Fig.5 illustrates has all of these features are integrated into the proposed method of propagation period simulation, details of the models for the incubation period, as illustrated in Fig.1, are skipped in the figure. In Fig.5, in order to distinguish the models previously proposed by the authors from those proposed by other researchers or institutes, the models followed by name(s) in parenthesis indicate the works of others.

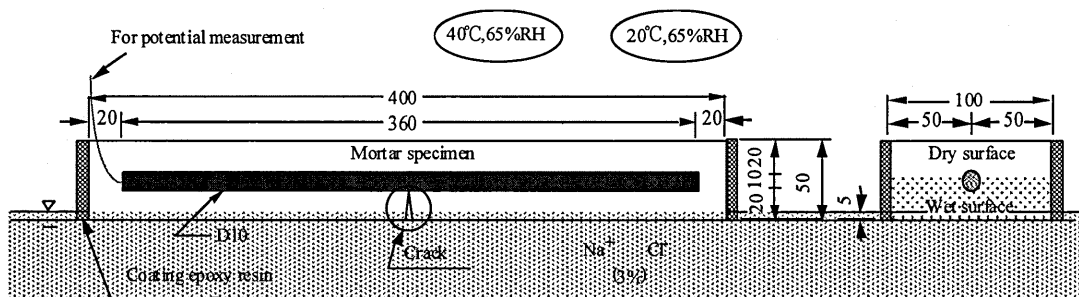


Fig.6 Layout and Setup of Specimen for Indoor Experiments

3. VERIFICATIONS

3.1 General

In order to verify the proposed numerical system, some indoor experiments were carried out for comparison with simulated results. These experiments were implemented under various experimental conditions. The material parameters used in the numerical analysis were derived from assumptions made in the constituent models based on the given mix proportion and environmental conditions. The availability of this numerical system is discussed by comparing the computed results for corrosion-related substances and electrochemical characteristics with the experimental values.

3.2 Outline of experiments

Eighteen reinforced mortar specimens (400 mm wide, 100 mm deep, and 50 mm high with a concrete cover of 20mm) were exposed under various conditions for 22 weeks. These indoor experiments were carried out by simulating a site with a high chloride concentration in the groundwater at the bottom surface and intense evaporation of water into the air from the top surface. The layout and setup of the experiments are illustrated in Fig.6. As this indicates, lower part of the specimen up to a height of 5mm was immersed in simulated groundwater; the chloride ion concentration in this simulated groundwater was close to 3% NaCl solution. To limit the movement of chlorides to the vertical direction only, all side surfaces of each specimen were coated by epoxy resin. The experimental conditions were varied as follows:

- water-cement ratio by weight: 40% and 50%
- exposure-temperature: 20°C and 40°C
- cracked specimens and uncracked specimens

Thus, there were a total of 6 experimental conditions, the results for each being taken as the average of 3 specimens. As for the type and specifications of the rebars, cement, admixtures, and aggregates, details are given in Table 1. The mix proportion is shown in Table 2. The various experimental conditions are listed in Table 3. The slump flow value and air content were measured at between 229~256 mm and 5.5~7.0%, respectively. To produce cracked specimens, a crack was introduced into the central zone at the bottom of the specimen by conducting three-point bending tests. Furthermore, for the method used to measure the corrosion potential, refer to the JCI committee report on repair methods for concrete structures²⁰⁾. Measurements

Table 1 Type and Required Specifications of Materials

Material	Type	Specification
Rebar	SD295,D10	JIS G 3112
Cement	Portland cement	JIS R 5210
Admixture	AE water reducing agent	JIS A 6206
Fine aggregate	Pit sand	JSCE concrete code (construction part) ¹⁹⁾
Coarse aggregate	Crashed limestone	
Water	Tap water	—

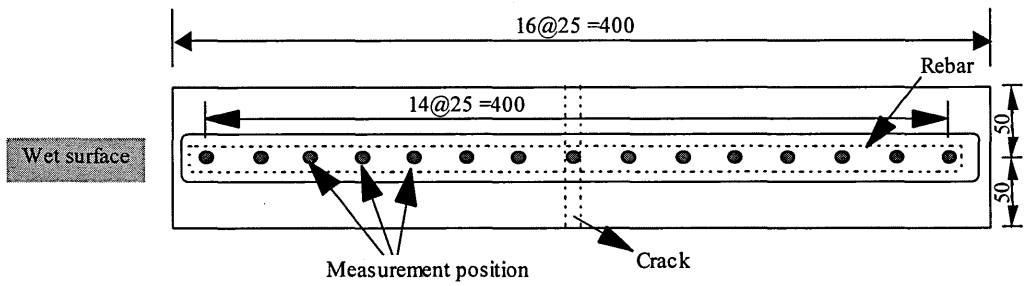


Fig.7 Illustration of Measurement Positions for Corrosion Potential

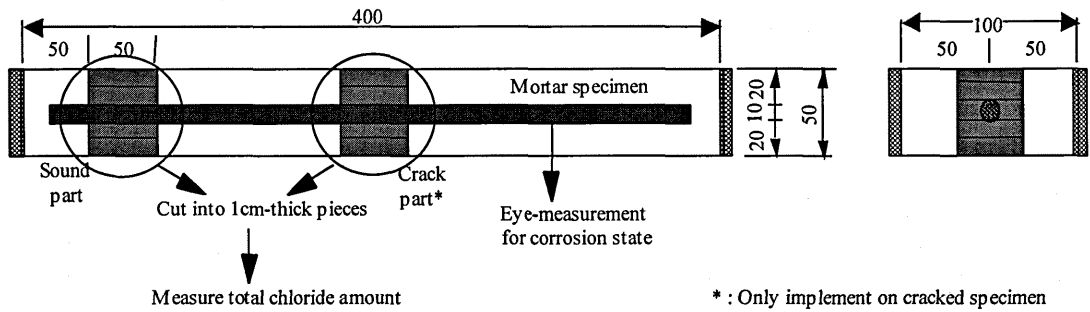


Fig.8 Illustration of sampling from specimen for measuring total chloride amount

Table 2 Mix Proportion of Mortar

W/C (%)	S/C (%)	Unit weight (kg/m ³)			
		W	C	S	AE water reducing agent
40	1.83	262	655	1201	C x 0.25wt%
50	2.50	262	526	1308	C x 0.25wt%

Table 3 Experimental Conditions

Case	1M	2M	3M	4M	5M	6M
W/C (%)	40	40	50	50	50	50
S/C (%)	1.83	1.83	2.50	2.50	2.50	2.50
Cracked specimen	yes	no	yes	yes	no	no
Width of crack (mm)	0.06	0.0	0.07	0.07	0.0	0.0
Temperature (°C)	40	40	40	20	40	20
Humidity (%RH)	65	65	65	65	65	65

were taken on the specimens on a wet surface, and the measurement positions are illustrated in Fig.7. As for the method of measuring the distribution of total chloride content, the standard procedure suggested by JCI⁽²¹⁾ (JCI-SC5) was used. The sampling points for measuring the distribution of total chloride content in cracked and uncracked specimens are shown in Fig.8.

3.3 Computational method

The above-described models used for simulation in the incubation and propagation periods result in a system of partial differential equations governing the corrosion process. A closed-form solution of this system of equations is impossible due to the interdependence of the models. However, the equations can be solved numerically in space as a boundary value problem and in time as an initial value problem by means of a two-dimensional finite element (FE) formulation. This FE formulation refers to the work of Balabanic⁽²²⁾ *et al.* Numerical solutions for this system of equations are achieved using the Crank-Nicholson method.

a) Chloride transport through crack surface

Regarding chloride transport through the crack surface in the specimens, the following assumptions were made. First, arrange the relationship between the flux (S_{crack}) through the crack surface and the flux (S_{sound}) through the sound surface as follows:

$$SS = S_{\text{crack}}/S_{\text{sound}} \quad (11)$$

where SS: the flux ratio between S_{crack} and S_{sound} , with a value greater than 1.0. Then, define the ratio of the surface area at the crack surface to the surface area at the sound surface as κ . The value of κ is also greater than 1.0. Here, it can be understood that the definitions of SS and κ are both dependent on the existence of cracks. Therefore, it can be assumed that the crack surface has the same influence level on the increased degree of the flux through the crack surface and the surface area at the crack surface, i.e. assuming $SS = \kappa$. Because of this assumption, S_{crack} can be taken as $S_{\text{crack}} = \kappa \cdot S_{\text{sound}}$. Generally speaking, the prevailing approach to chloride transport through a crack surface is to set the diffusion coefficient at the crack surface as several times the value of the diffusion coefficient at the sound surface (e.g., the work of Ishida²³ *et al.*), though this lacks substantial support in terms of the physical process. On the contrary, although there is some difficulty in clarifying the exact values of SS and κ , the reasonableness of these assumptions appear to be supported by the hypothetical physical process. Thus, this model is introduced in calculating chloride transport through the crack surface. As for the value of κ , it is estimated by fitting the calculated total chloride context at the crack surface to the experimental results, giving a ranged from 1.5 to 5.0.

b) Choice of simulation parameters

The essential parameters used for each simulation case are listed in Table 4. The resistivity of the mortar specimens was calculated according to the work of Saeki²⁴ *et al.*, in which it was experimentally found that the resistivity depends on the degree of hydration and carbonation, the water content, and temperature. From these findings, resistivity is defined as a multiplication function of these factors.

4. RESULTS AND DISCUSSION

4.1 State of rebar corrosion

In order to determine whether if the rebars in the specimens were corroding or not, specimens were split open at the 10th, 16th, and 22nd week to check their corrosion state by eye. The results of this are shown in Table 5. Regardless of the mix proportion and exposure environment, the lower surface (i.e. the surface toward the groundwater) of the rebars in all cracked specimens was found to be corroding after 10 weeks of exposure. Further, the upper surface (i.e. the surface toward the drying face) of the rebars in all cracked specimens except case 4M was also found to be corroding after 10 weeks of exposure. Secondly, among the uncracked specimens, case 5M was found to be corroding after 10 weeks of exposure while cases 2M and 6M were found to be corroding after 22 weeks of exposure. The simulated results of the variation of maximum ratio of [Cl⁻] and [OH⁻] along the rebars with respect to time for each case are shown in Fig.9. Fig.9 demonstrates substantial agreement in the start of corrosion with the experimental results when the chloride threshold value given in Eq.(5) is introduced.

4.2 Penetration of chloride ion

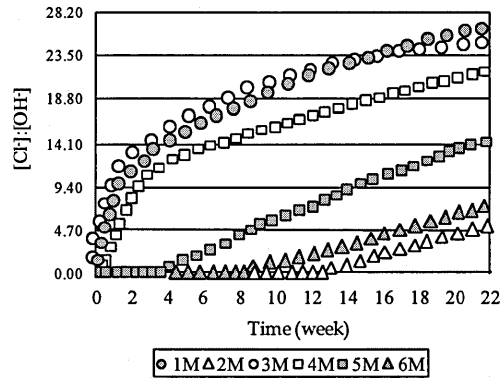


Fig.9 Maximum [Cl]:[OH] along Rebar with respect to time

Table 4 Material Parameters for Simulation

Parameters		Case	1M	2M	3M	4M	5M	6M
Diffusion coefficient (10 ⁻³ cm ² /day)	Water	surface	83.6	83.6	145	66.2	145	66.2
		inner	22.6	22.6	46.0	18.1	46.0	18.1
	Chloride	surface	4.24	4.24	7.16	2.04	7.16	2.04
		inner	3.53	3.53	5.97	1.70	5.97	1.70
Resistivity (ω)		(10 ⁴ Ω-cm)	2.70	2.70	2.90	7.40	2.90	7.40
Surface increased ratio (κ)		Sound surface	1.0	1.0	1.0	1.0	1.0	1.0
		Cracked surface	1.5	0.0	1.5	1.5	0.0	0.0

Table 5 Observed Corrosion of Rebars

Parameters		Case	1M	2M	3M	4M	5M	6M
Diffusion coefficient (10 ⁻³ cm ² /day)	Water	surface	83.6	83.6	145	66.2	145	66.2
		inner	22.6	22.6	46.0	18.1	46.0	18.1
	Chloride	surface	4.24	4.24	7.16	2.04	7.16	2.04
		inner	3.53	3.53	5.97	1.70	5.97	1.70
Resistivity (ω)		(10 ⁴ Ω-cm)	2.70	2.70	2.90	7.40	2.90	7.40
Surface increased ratio (κ)		Sound surface	1.0	1.0	1.0	1.0	1.0	1.0
		Cracked surface	1.5	0.0	1.5	1.5	0.0	0.0

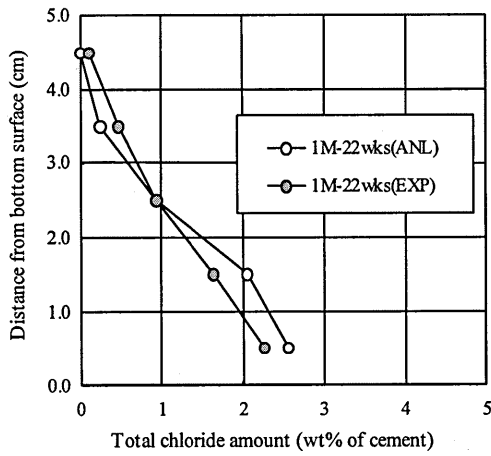


Fig.10 (a) Total Chloride Content in Cracked Specimen (1M)

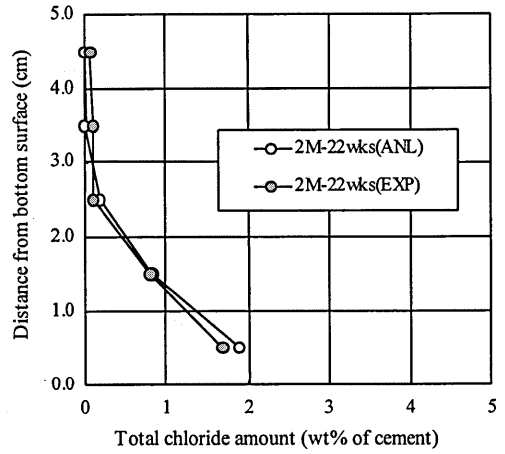


Fig.11 (a) Total Chloride Content in Cracked Specimen (2M)

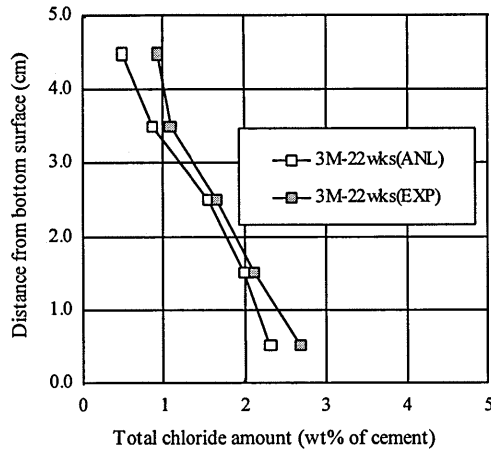


Fig.10 (b) Total Chloride Content in Cracked Specimen (3M)

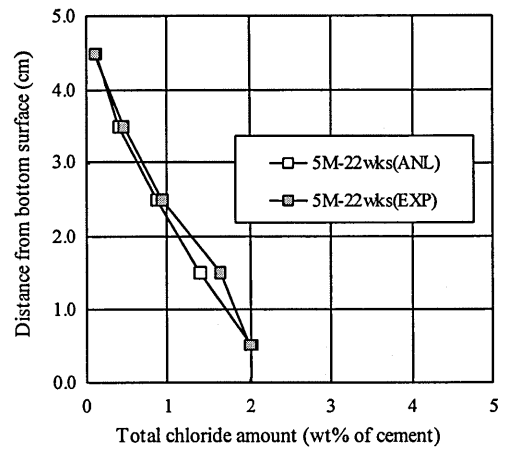


Fig.11 (b) Total Chloride Content in Cracked Specimen (5M)

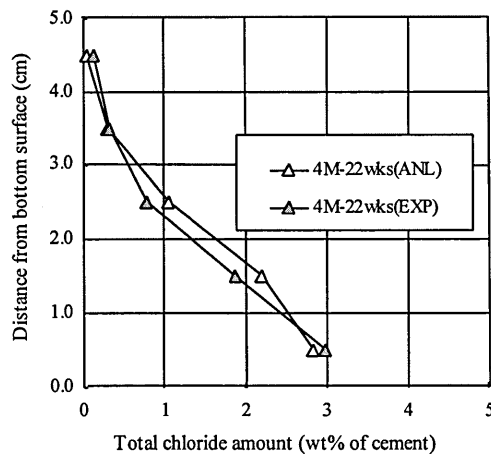


Fig.10 (c) Total Chloride Content in Cracked Specimen (4M)

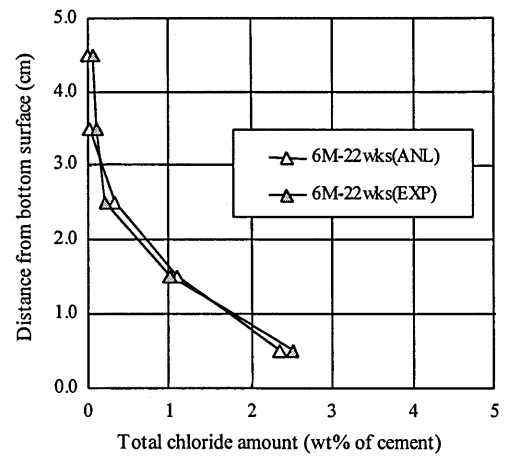


Fig.11 (c) Total Chloride Content in Cracked Specimen (6M)

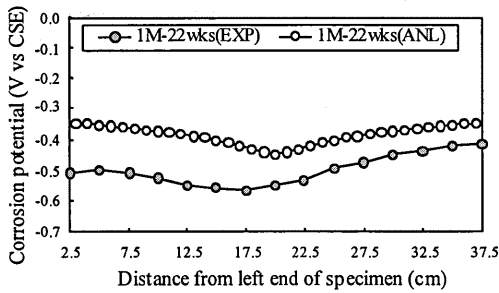


Fig.12 (a) Corrosion Potential Distribution in Cracked Specimen (at Wet Surface) (1M)

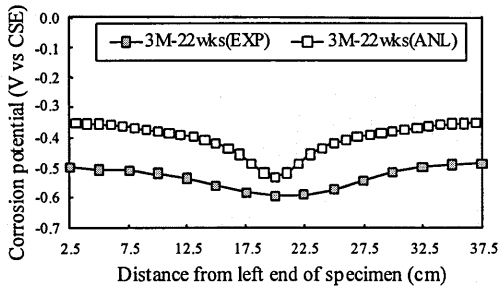


Fig.12 (b) Corrosion Potential Distribution in Cracked Specimen (at Wet Surface) (3M)

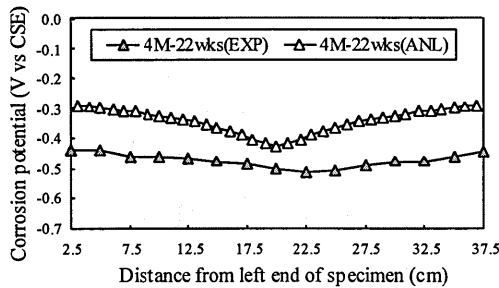


Fig.12 (c) Corrosion Potential Distribution in Cracked Specimen (at Wet Surface) (4M)

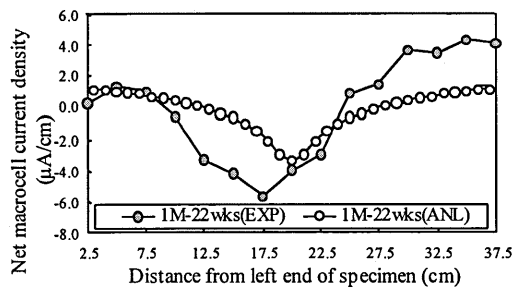


Fig.13 (a) Macrocell Current Density in Cracked Specimen (Converted from Corrosion Potential) (1M)

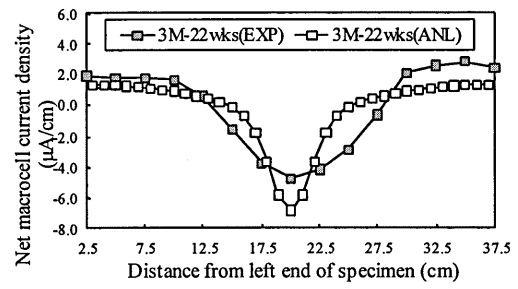


Fig.13 (b) Macrocell Current Density in Cracked Specimen (Converted from Corrosion Potential) (3M)

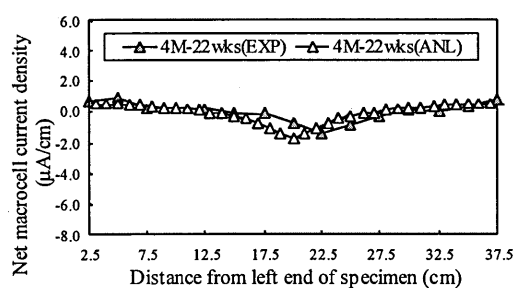


Fig.13 (c) Macrocell Current Density in Cracked Specimen (Converted from Corrosion Potential) (4M)

Regarding the penetration of chloride ions, the experimental results for the distribution of total chloride content in cracked and uncracked specimens at the 22nd week are reported in Fig.10 and Fig.11, respectively; these are the cases labeled EXP. It is clearly seen that the upward movement of chloride ions in cracked specimens is more significant than in uncracked specimens. Further, based on the parameters given in Table 3 and the algorithms for calculating the transport of corrosion-related substances, the simulated distributions of total chloride content in cracked specimens 1M, 3M, and 4M are shown in Fig.10 (a), (b), and (c) while, for uncracked specimens 2M, 5M, and 6M, the results are given in Fig.11 (a), (b), and (c). These comparisons indicate agreement between experimental and simulated results, thus verifying this availability of the numerical system for predicting the transport of corrosion-related substances in concrete.

4.3 Corrosion potential

Regarding the distribution of corrosion potential, the experimental results for cracked specimens are shown in Fig.12 (a)-(c). It is clear that the value of corrosion potential near a preexisting crack in the specimen is lower than that where there is no cracks, and the reason for this is related to the initiation of corrosion at cracks. Besides, based on the electrochemical models, including the microcell and macrocell models, as well as the FEM

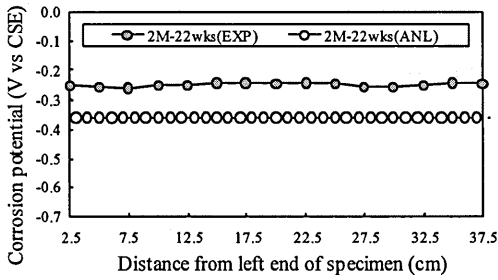


Fig.14 (a) Corrosion Potential Distribution in Uncracked Specimen (at Wet Surface) (2M)

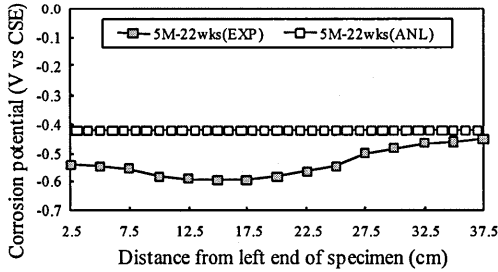


Fig.14 (b) Corrosion Potential Distribution in Uncracked Specimen (at Wet Surface) (5M)

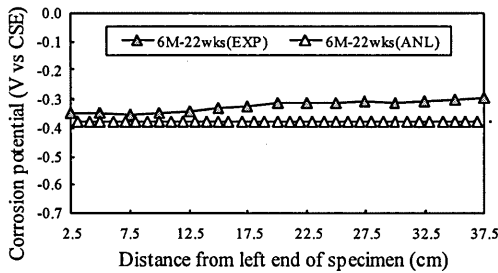


Fig.14 (c) Corrosion Potential Distribution in Uncracked Specimen (at Wet Surface) (6M)

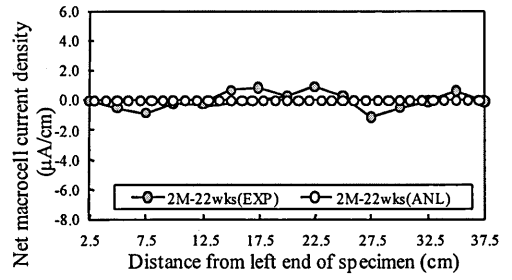


Fig.15 (a) Macrocell Current Density in Uncracked Specimen (Converted from Corrosion Potential) (2M)

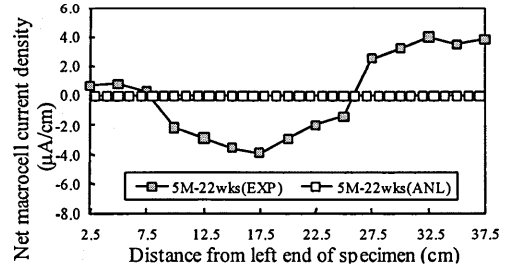


Fig.15 (b) Macrocell Current Density in Uncracked Specimen (Converted from Corrosion Potential) (5M)

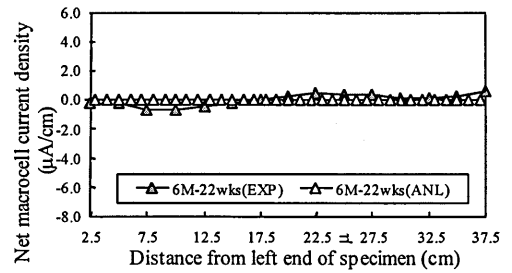


Fig.15 (c) Macrocell Current Density in Uncracked Specimen (Converted from Corrosion Potential) (6M)

formulation of the Laplace equation, the simulated results for the distribution of corrosion potential over the wet surface of a cracked specimen are also shown in Fig.12 (a)-(c) respectively. The discrepancy between the experimental and simulated results in Fig.12 (a)-(c) may be ascribed to the ambiguity in describing the quantitative relationship between the electro-chemical characteristics (e.g. the pitting potential of steel in concrete, the Tafel slope, and the resistivity) and the corrosion-related substances including chlorides, moisture, and oxygen. If the precise relationship between them could be well described, it is believed that the deviation between experimental and simulated results would diminish.

4.4 Macrocell current density

Based on the measured (or simulated) corrosion potential, the net macrocell current density can be converted. The results for both cases are given in Fig.13 (a)-(c) for cracked specimen; here, a positive value indicates a cathode while a negative value indicates an anode. From these figures, it can be inferred that there should be serious corrosion at the central section of the rebars in the cracked specimens, because a large negative value can be seen near the middle of the rebars due to the preexisting cracks. According to observations of the split specimens, the real corrosion domain was found to correspond almost exactly with the distribution of net macrocell current density. This discussion makes it clear that the distribution of net macrocell current density is helpful in locating the domains under corrosion domains, i.e. the location of anodes.

4.5 Influence of cracks

The discussions above demonstrate that the existence of cracks introduced by three-point bending tests has a significant influence on corrosion state of rebars. They reduce corrosion resistance around the crack and encourage early corrosion of rebars near the crack. By assuming a proper model for the transport of corrosion-related substances through the crack and combining the proposed electrochemical models, agreement is achieved between experimental and simulated results for the distribution of total chloride content, corrosion potential, and net macrocell current density, as shown in Fig.10, Fig.12, and Fig.13. On the other hand, corresponding comparisons for uncracked specimens are given in Fig.11, Fig.14, and Fig.15. These figures lead to the following observations. First, as shown in Fig.11, with appropriate parameters for predicting the transport of corrosion-related substances, their distributions can be predicted achieved. Also, the simulated distributions of corrosion potential for uncracked specimens indicate that corrosion starts at the 22nd week, as shown in Fig.14. Nevertheless, there is a deviation between experimental and simulated results. The reasons for this deviation may not be limited to these mentioned in connection with cracked specimens, but might also include the homogeneity of transgression of corrosion-related substances introduced in the process of simulation for uncracked specimens. In fact, although there is no need to include a model for the transport of corrosion-related substances through cracks in uncracked specimens, uncertainty in the location of anode(s) gives rise to a difficulty in simulating the net macrocell current. That is to say, in the process of simulation, the heterogeneity (i.e. the existence of cracks) of transgression of corrosion-related substance in cracked specimens makes it easy to specify the location of the anode. On the other hand, the homogeneity (i.e. absence of cracks) of transgression of corrosion-related in uncracked specimens make it difficult to specify the location of the anode. Consequently, as shown in Fig.15, the simulated results indicate there was no net macrocell current density while the experimental results point to corrosion in the case of uncracked specimens after 22 weeks of exposure. Moreover, the location of anode(s) at which corrosion occurs in uncracked specimens, as observed in the experimental results, cannot be predicted by the simulations.

5. CONCLUDING REMARKS

On the basis of algorithms explained in the earlier sections and the results of an experimental verification, the following conclusions can be drawn from this paper:

- (1) The ability to trace time-dependent chloride-induced macrocell corrosion is recognized.
- (2) There is a further need to verify the quantitative relationship between electrochemical characteristics and corrosion-related substances.
- (3) In the process of simulation, there is a need to overcome the uncertainty in the location of anode(s) in homogeneous specimens (with no cracks). This also warrants further investigation.

References

- [1] Miyagawa, T., Masuda, Y., Takewaka, K., Moriwake, A., Ueda, T.: Proper application of rehabilitation methods for concrete structures deteriorated by chloride-induced corrosion, Proc. 2nd Int'l RILEM/CSIRO/ACRA Conference on Rehabilitation of Structures, pp.557-568, Sep. 1998.
- [2] Takewaka, K., Hamada, H. and Ohta, T.: Deterioration Mechanism and Rehabilitation on Concrete Structures, Concrete Journal, JCI, Vol.36 No.7, pp.6-10, Jul. 1998 (in Japanese).
- [3] Maruya, T. and Hsu, K.L.: Numerical simulation on Cl⁻, moisture, O₂ and CO₂ in concrete, 42nd Proc. of Japan Congress on Materials Research, Sep. 1998 (in Japanese).
- [4] Shimomura, T. and Maekawa, K.: Analysis of the drying shrinkage behavior of concrete using a micromechanical model based on the micropore structure of concrete, Mag. Conc. Res., Vol.49 No.181, pp.303-322, Dec. 1997.
- [5] Saeki, T., Ohga, H. and Nagataki, S.: Mechanism of carbonation and prediction of carbonation process of concrete, Proc. of JSCE, No.414/V-12, pp.99-108, Feb. 1990 (in Japanese).
- [6] Hsu, K.L., Takeda, H. and Maruya, T.: Numerical simulation on migration of oxygen and carbon dioxide in concrete, Proc. JCI, Vol.20 No.1, pp.769-774, 1998.
- [7] Maruya, T., Tangtermsirikul, S. and Matsuoka, Y.: Modeling of chloride ion movement at the surface layer of hardened concrete, Proc. of JSCE, No.585/V-38, pp.79-95, Feb. 1998 (in Japanese).

- [8] Saetta, A.V., Scotta, R.V. and Vitaliani, R.V. : Analysis of chloride diffusion into partially saturated concrete, *ACI Materials J.*, V-90, No.5, pp.441-451, 1993.
- [9] Japan Conc. Inst., Technical report on material design and performance of concrete structures, Symposium on Material Design and Performance of Concrete Structures, pp.162-180, May 1999 (in Japanese).
- [10] Hsu, K.L. and Maruya, T.: Modeling time-dependent response of chloride-induced macrocell corrosion of steel in concrete, *Proc. JCI*, Vol.21, No.2, pp.1009-1014, 1999.
- [11] Okada, T.: Two-step initiation theory of pitting corrosion in passive metals, *Boshoku Gijutsu*, Vol.36, pp.787-794, 1987.
- [12] Bird, H.E.H., Pearson, B.R. and Brook, P.A.: The breakdown of passive films on iron, *Corrosion Sci.*, Vol.28, No.1, pp.81-86, 1988.
- [13] Glass, G.K. and Buenfeld, N.R.: The presentation of the chloride threshold level for corrosion of steel in concrete, *Corrosion Science*, Vol.39, No.5, pp.1001-1013, 1997.
- [14] Yonezawa, T., Ashworth, V. and Procter, R.P.M.: The mechanism of fixing Cl⁻ by cement resulting in the transformation of NaCl to NaOH, *Proc. 8th International Conference on Alkali-Aggregate Reaction*, pp.153-160, 1989.
- [15] Lambert, P., Page, C.L. and Vassie, P.R.W.: Investigations of reinforcement corrosion. 1. The pore electrolyte phase in chloride-contaminated concrete, *Material & Structures*, 24, pp.243-252, 1991.
- [16] Japan Conc. Inst., Technical report on repair methods of concrete structure (III), pp.198-212, Oct. 1996 (in Japanese).
- [17] Japan Conc. Inst., Technical report on repair methods of concrete structure (III), pp.226-232, Oct. 1996 (in Japanese).
- [18] Maeda, K.: Study on corrosion content of steel bar due to cracking of concrete cover using electrical corrosion test, *Summaries Tech. Papers Ann. Meeting Archit. Inst. Japan*, pp.147-148, Sep. 1983 (in Japanese).
- [19] Japan Society of Civil Engineers., Standard specification for concrete structures [construction], 1996 (in Japanese).
- [20] Japan Conc. Inst., Technical report on repair methods of concrete structure, p.35, Oct. 1992 (in Japanese).
- [21] Japan Conc. Inst., Test methods and specifications for corrosion and anticorrosion of concrete structures, 1987 (in Japanese).
- [22] Balabanic, G., Bicanic, N. and Durekovic, A.: Mathematical modeling of electrochemical steel corrosion in concrete, *J. Eng. Mech.*, Vol.122, No.12, pp.1113-1122, Dec. 1996.
- [23] Ishida, T., Chaube, R.P., Kishi, T. and Maekawa, K.: An integrated computational system of mass/energy generation and transport, and material mechanical behavior, *Proc. JCI*, Vol.20 No.2, pp.233-238, 1998 (in Japanese).
- [24] Saeki, T., Ohga, H. and Nagataki, S.: Quantitative estimation of steel corrosion in mortar due to carbonation, *Proc. of JSCE*, No.532/V-30, pp.55-66, Feb. 1996 (in Japanese).